Hybrid Reduction of a Bipedal Walker from Three to Two Dimensions

Robert D. Gregg
Electrical Engineering and Computer Sciences
University of California, Berkeley
bobbyg@berkeley.edu

Graduate Mentor: **Aaron D. Ames**
Research Supervisor: **Dr. Jonathan Sprinkle**
Faculty Mentor: **Prof. S. Shankar Sastry**

July 29, 2005

Summer Undergraduate Program in
Engineering at Berkeley (SUPERB) 2005

Department of Electrical Engineering and Computer Sciences
College of Engineering
University of California, Berkeley

Hybrid Reduction of a Bipedal Walker from Three to Two Dimensions

Robert D. Gregg

Abstract

Because the complexity of bipedal walking robots doubles when increasing a model's dimensions from two to three, many previously established analytical techniques are computably impractical for three-dimensional models. If bipedal walkers can be analyzed in three dimensions, we can more accurately reproduce the humanoid walking that we observe in our three-dimensional world. This paper offers a systematic approach to reducing a 3D biped model into two dimensions, on which 2D analytical methods can be used, such as numerical analysis to find the limit cycles that result in asymptotically stable walking. The hybrid reduction consists of five stages: hybridization of the robot's motion, Lagrangian formulation of the continuous dynamics, formulation of the discrete impact transition map, dependency simplification, and the Lagrangian reduction. We present the results of this method's application on a simple compass-gait biped using a fixed angle simplification and Routhian reduction. We show that the reduced model is related to the analogous 2D model by a computable augmented potential component. The model is easily brought back into 3D using the Routhian relation and can be implemented in a simulation for analysis. Moreover, we provide supporting evidence for periodicity in the reconstructed 3D model given periodicity in the reduced 2D model. The outcome of this paper is a general framework by which previously established techniques can be applied to three-dimensional biped models.

1 INTRODUCTION

1.1 Analysis of Planar Walkers

Bipedal walking robots have been an area of interest for the past few decades. The implications of understanding such locomotion are great due to its human application. The potential for improving prosthetic limbs, navigating non-flat terrestrial surfaces, and creating efficient locomotive mechanisms are among the many incentives that drive research in this field.

A simple bipedal walker is very similar to the dynamical system of a double-pendulum (a fixed-pivot inverted pendulum and a moving-pivot pendulum). However, bipeds are non-trivial because of the impulse-effects upon foot impact. The motion of the biped during the single-support phase is continuous and easily modeled, but at the instantaneous double-support phase (foot impact) the leg velocities are discontinuous. The non-smooth hybrid dynamics can be described by continuous ordinary differential equations, which are reset by a discrete event. The field of hybrid systems is one with many open problems, and analysis on bipedal walking is a fantastic example.

Most studies to date have focused on planar bipeds, which are models fixed in two dimensions (within the sagittal plane). One class of planar bipeds consist of those with actuation. These robots have been shown to walk on level surfaces and inclines, and even various forms of jumping have been achieved [5]. In order to guarantee steady walking for these feedback controlled systems, asymptotic stability for an under actuated biped is proven in [10, 11].

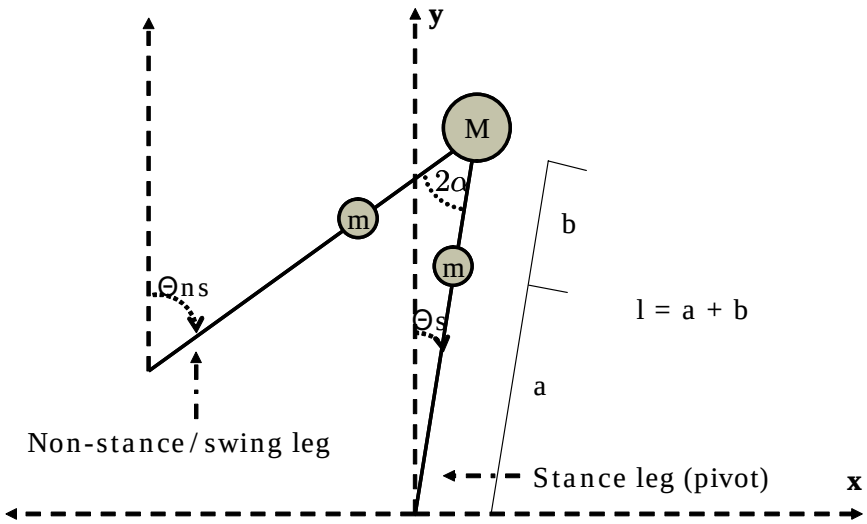

Figure 1. Structure of Two-Dimensional Bipedal Walker

Moreover, many have studied the passivity paradigm of bipedal robot control. Passive bipeds are unactuated and walk down slight slopes, harnessing the natural forces of gravity to power its dynamics. Many forms of passivity-based control produce bipedal walking with periodic gaits, also known as limit cycles [21, 8]. One such technique for finding limit cycles is trajectory sensitivity analysis, which we will later use in this paper [12]. Steady gaits are made slope invariant using potential energy shaping control, a generalization of the very sensitive slope parameter [22]. A passive walker with telescopic legs is shown in [18], and one with revolute knees is shown in [7]. In this paper, we are interested in analysis of the passive class of bipeds.

It is important to note that although many analytical methods have been demonstrated on different forms of bipeds, most have been restricted to planar models. If we are to increase our understanding of human-like walking, we must study three-dimensional models that more accurately reproduce what we see in our three-dimensional world. Kuo shows passive limit cycles in three dimensions by using a feedback controller to stabilize the lateral motion [14]. Furthermore, in [23] a general case of an n degrees-of-freedom 3D biped is shown to achieve slope-invariant passive limit cycles using controlled symmetry of a closed-loop system. We examine a bipedal model with an open-loop system. Michael Coleman examines a straight-legged, point-foot 3D walker, but he only finds almost-stable walking gaits due to the complexity of the analysis [6]. A passive 3D model with two legs, knees, and specially shaped feet is implemented in [7], but little insight is offered into systematically analyzing such a complicated model. The next sections will explore the problem of 3D analysis and propose our solution.

1.2 Scaling Complexity from 2D to 3D

1.2.1 Two-Dimensional Compass Gait Biped

In order to explain the problem of scaling complexity when going from 2D to 3D, we first introduce our application's model. Many different bipedal robot structures have been used in previous work, the most prevalent being the compass-gait biped. A very simple compass-gait biped with leg masses at the feet is presented in [8], whereas a more general compass-gait biped with a torso is presented in [10]. We use the structure from [9], which is a simple compass-gait biped with generalized leg mass positions. The two-dimensional version is

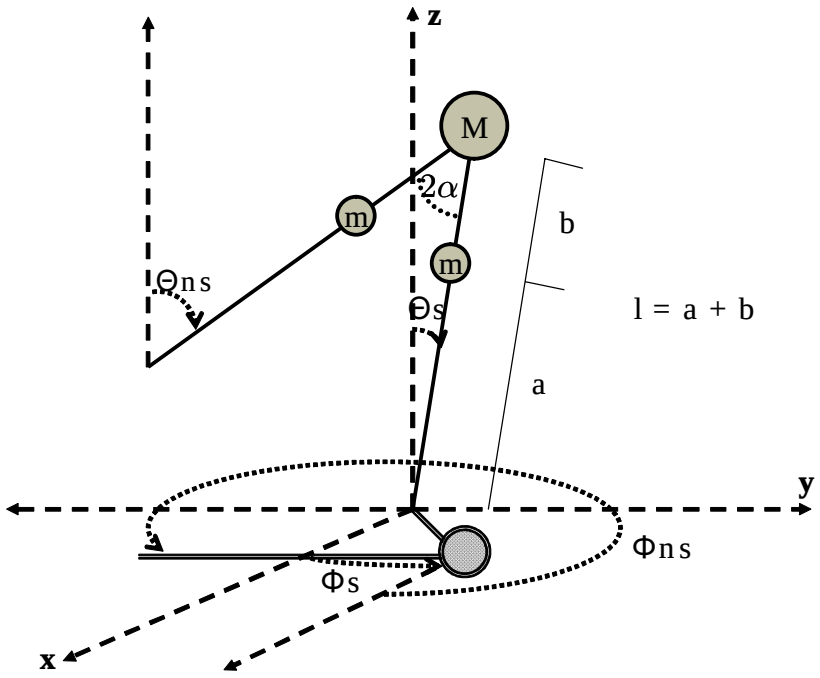

Figure 2. Structure of Three-Dimensional Bipedal Walker

shown in Fig. 1.2.1. The robot's motion is described by four state variables, the angular positions of the stance and non-stance/swing legs and their time-derivatives. The parameters and their descriptions are:

- M is the point-mass at the hip
- m is the point-mass of each leg (usually smaller than the hip mass)
- a is the distance between the foot and point-mass for each leg
- b is the distance between the point-mass and hip for each leg
- l is the total length of each leg ($l = a + b$)
- γ is the slope angle (small, $< 5°$)
- α is the half-angle between the legs in the sagittal plane (equation 3)
- θ_{ns} is the clockwise angle of the non-stance/swing leg from the z-axis in the sagittal plane
- θ_s is the clockwise angle of the stance/pivot leg from the z-axis in the sagittal plane

1.2.2 Three-Dimensional Compass Gait Biped

The same robot structure in three dimensions is shown in Fig. 1.2.2. In order to describe the robot's motion, each leg needs an angular position state relative to both the x-y plane (ϕ) and y-z plane (θ). This results in an eight-dimensional phase space: four position variables along with the four corresponding velocities. The 3D model uses all the 2D parameters, plus the following:

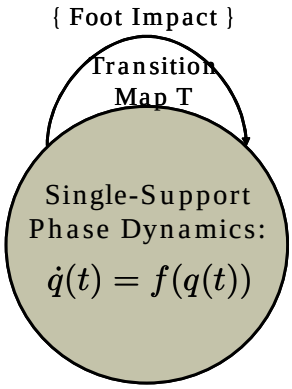

Figure 3. Hybridization of Bipedal Robot Motion

- ϕ_{ns} is the counter-clockwise angle of the non-stance/swing leg from the y-axis in the lateral plane
- ϕ_s is the counter-clockwise angle of the stance/pivot leg from the y-axis in the lateral plane

Numerical analysis and searches on a four-dimensional phase space ($S^2 \times \Re^2$) already takes hours of computation time. The same methods on an eight-dimensional phase space ($S^4 \times \Re^4$) would be computably impractical.

In this paper, we present a process of hybrid reduction to simplify the model. We exploit symmetries in the model's dynamics in order to reduce the system into two dimensions. This allows previously established techniques to be applied to a familiar four-dimensional phase space. The reduced 2D model is uniquely brought back into three dimensions, and we present supporting evidence that characteristics of the reduced 2D model also apply to the reconstructed 3D model.

2 HYBRID REDUCTION FROM 3D TO 2D

2.1 Hybridization of Robot Motion

A hybrid system is described by a directed graph of continuous dynamical systems that are switched at discrete events. Our hybrid bipedal walker will be defined by a discrete state, edge, domain, guard, transition map, and flow [1]. The discrete state describes the continuous dynamics of the single-support phase. The edge is a reset transition for the state. The domain D is the phase space of the robot's configuration ($S^4\Re^4$ for the full-order model), and the guard $G \in D$ at foot impact, i.e.:

$$\theta_{ns}(t) + \theta_s(t) = -2\gamma \text{ and } \theta_{ns}(t) > 0 \tag{1}$$

The reset map T at collision is discussed in the next section. Finally, the flow

$$\Phi_t(x_0), \text{ with } x_0 \in D$$

is the solution to the ordinary differential equations that describe the state. This is found using numerical analysis.

Given a hybrid system, it is important to define a solution. First, the flow is needed for the continuous dynamical system. A solution to the ODE:

$$\dot{x} = f(x)$$

is

$$\Phi_t(x_0) \text{ s.t. } \frac{d}{dt}(\Phi_t(x_0)) = f(\Phi_t(x_0))$$

Now, the solution to our hybrid system is:

$$S = (\tau, \chi, \Phi) \tag{2}$$

where

$$\tau = \{t_0, t_1, ..., t_k, ...\} = \{t_i\}_{i \in \mathbb{N}}$$
$$\chi = \{x_0, x_1, ..., x_k, ...\} = \{x_i\}_{i \in \mathbb{N}}$$

and the solution $\Phi_t(x_i)$ to the continuous dynamics with initial conditions (x_i, t_i) satisfy:

1. $\Phi_{t_{i+1}-t_i}(x_i) \in G$
2. $x_{i+1} = T(\Phi_{t_{i+1}-t_i}(x_i))$

Moreover, a periodic solution to the hybrid system is:

$$S_p = \{\chi, \tau, \Upsilon\} \text{ s.t. } x_i = x_0, \forall i$$

which implies that

$$t_i - t_{i-1} = t_1 - t_0, \forall i$$

2.2 Discrete Foot Impact

When the swing foot hits the slope, the system enacts a reset transition. The angular positions undergo a change of coordinates: the former swing leg becomes the new pivot leg, and the former stance leg becomes the new swing leg. The transition of the angular positions in the sagittal plane is described by:

$$\theta^+ = P\theta^-$$

with:

$$P = \begin{pmatrix} 0 & 1 \\ 1 & 0 \end{pmatrix}$$

The angular positions of the lateral plane are reset by a different map, but because this 3D model is to be reduced into 2D, we will present the ϕ reset map when we discuss 3D reconstruction. The same will be done with $\dot{\phi}$.

At foot impact, angular momentum is conserved, so the normal motion of the swing foot is transferred to the tangential motion of the pivot foot. This transfer of mechanical energy is guided by the system's reset map, which is composed of impact equations. Various techniques exist for modeling impulsive impacts. In [10], the equations are derived with generalized coordinates using the rigid body collision methods of Hurmuzlu and Marghitu [13]. We use the impact equations of [9] in order to be consistent with the robot model:

$$\dot{\theta}^+ = H(\alpha)\dot{\theta}^-$$

where

$$\theta_s(t) - \theta_{ns}(t) = 2\alpha, \forall t \tag{3}$$

and $H(\alpha)$ is given in Appendix (19).

Combining these two transition maps, the reduced model's reset map is described by:

$$x^+ = T_r(\alpha)x^- \tag{4}$$

where $x = (\theta_{ns}, \theta_s, \dot{\theta}_{ns}, \dot{\theta}_s)^T$, and

$$T_r(\alpha) = \begin{pmatrix} P & 0 \\ 0 & H(\alpha) \end{pmatrix} \tag{5}$$

2.3 Lagrangian Continuous Dynamics

The dynamics of the single-support phase are described by ordinary differential equations. In order to derive these ODEs, we model the continuous system using the Lagrangian formulation. The Lagrangian L accounts for all energy of a given system, and by definition satisfies [19, 4]:

$$\frac{d}{dt}\frac{\partial L}{\partial \dot{q}_i} - \frac{\partial L}{\partial q_i} = 0, \forall i \in \{\text{indices of all position states}\} \tag{6}$$

For example, the following equation describing the energy of a free-falling ball of mass m is a Lagrangian:

$$L(y(t), \dot{y}(t)) = K - V = \frac{1}{2}m\dot{y}(t)^2 - mgy(t)$$

Taking the partials and derivative,

$$\frac{\partial L}{\partial y(t)} = -mg$$

$$\frac{d}{dt}\frac{\partial L}{\partial \dot{y}(t)} = m\ddot{y}(t)$$

and using the definition of Lagrangian (6), we get the simplified expression $-g = \ddot{y}(t)$. Since this is a free-falling ball, we know that the downward acceleration is indeed $g = 9.8\frac{m}{s^2}$. This, albeit a trivial example, is the derivation of the falling ball's equation of motion.

The Lagrangian formulation of our full-order walker's dynamics is significantly more complicated, and is given in Appendix (24). From this Lagrangian, the equations of motion are derived using the same technique as above. In general form, the system of equations is [8, 9, 10]:

$$M(q)\ddot{q} + F(q, \dot{q})\dot{q} + g(q) = 0 \tag{7}$$

where $q = (\theta_{ns}, \theta_s, \phi_{ns}, \phi_s)^T$. The 4×4 matrix $M(q)$ contains the kinematic terms, and the 4×4 matrix $F(q)$ contains the centrifugal and Coriolis terms. The 4×1 vector $g(q)$ holds the gravitational torques, which are dependent only on the θ variables.

In order to simplify the equations, the system can be described in normalized form:

$$ma^2(M(q)\ddot{q} + F(q, \dot{q})\dot{q} + \frac{1}{a}g(q)) = 0 \tag{8}$$

At this point, we introduce the ratio terms $\beta = \frac{b}{a}$ and $\mu = \frac{M}{m}$. The normalized components are given in Appendix (28, 29, 30). The rest of this paper will use normalized form whenever appropriate.

2.4 Dependency Simplification

The model derived in the previous section, composed of four lengthy equations, is very complicated. Clearly, numerical searches on this system would be impractical. Moreover, we do not have the three-dimensional impact equations to reset the hybrid system. All this demonstrates the need for a system reduction, such as Routhian reduction. However, in order to do Routhian reduction, the system's Lagrangian must have cyclic variable(s). A cyclic variable q_i is a position state that is independent of the Lagrangian:

$$\frac{\partial L}{\partial q_i} = 0 \tag{9}$$

Once cyclic variables are found, the corresponding velocity states are replaced in terms of the remaining variables and the conserved quantities.

The Lagrangian from the previous section, given in Appendix (24), has no cyclic variables. Therefore, we perform a dependency simplification on the system by constraining certain variables. Various constraints were attempted.

2.4.1 Limit as leg-mass ratio μ goes to infinity

This simplified model is equivalent to an inverted pendulum with a massless, moving-pivot pendulum. By dividing rows two and four of (8) by μ, the dynamics equations that are influenced by the mass ratio become dependent on the inverse of μ. Taking the limit as μ goes to infinity, we get a greatly simplified system. However, the resulting matrix $M(q)$, which is used to build the Lagrangian, has no independent angular positions.

2.4.2 Limit as leg-length ratio β goes to infinity

This simplified model is equivalent to a robot with leg masses at the foot, similar to the 2D biped of [8]. By dividing the entire system of (8) by β^2, the dynamics equations become dependent on the inverse of β. Taking the limit as β goes to infinity, we get a marginally simplified system. Once again, the resulting matrix $M(q)$ has no independent angular positions.

2.4.3 Fix half-angle α as a constant

This simplification results in a biped model that walks like a true rotating compass. The constraint and equation (3) result in a sagittal angle being expressed in terms of the other. We set

$$\theta_s(t) = \theta_{ns}(t) + 2\alpha$$

for some constant 2α. It then follows that:

$$\dot{\theta}_s(t) = \dot{\theta}_{ns}(t)$$

Obviously, with this substitution the Lagrangian is independent of one position state, but because the corresponding velocity state is also independent, the simplification is not useful for Routhian reduction. It does, however, eliminate a dimension from the system of equations (now three) and two dimensions from the phase space (now six). This specific model may be the subject of future studies.

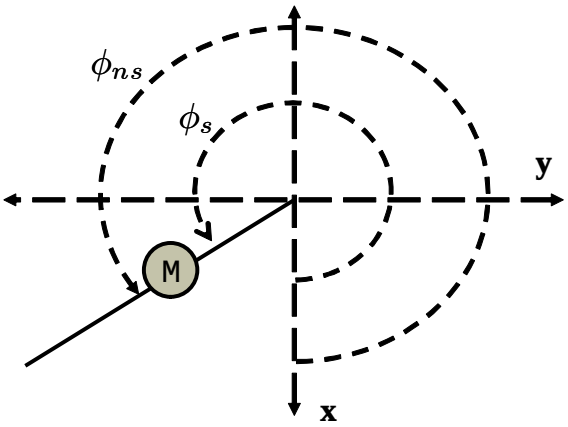

(a) Outstretched after step, slow linear velocity

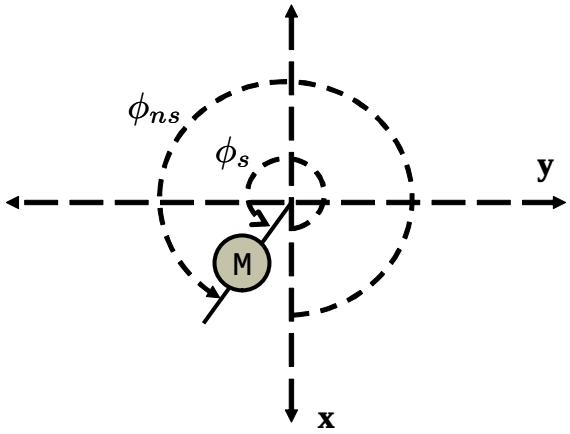

(b) Folding inwards, increasing velocity

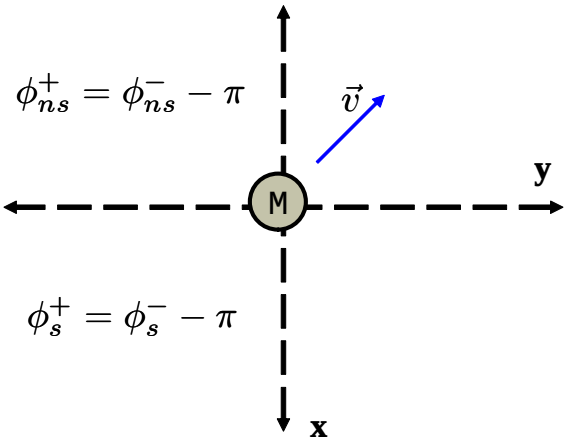

(c) Completely folded, maximum linear velocity

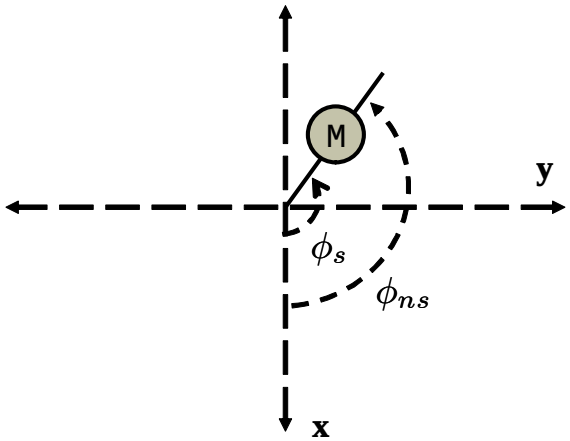

(d) Unfolding, decreasing velocity

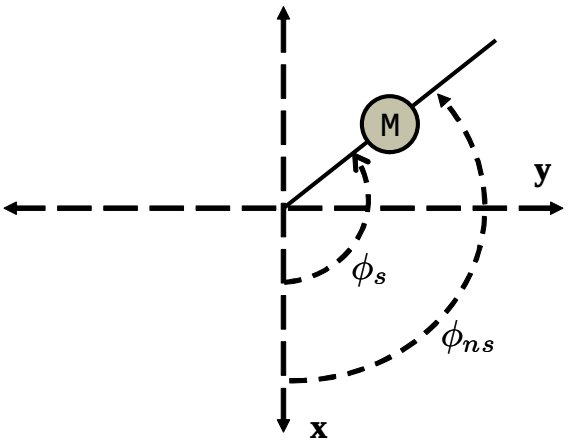

(e) Outstretched for step, slow linear velocity

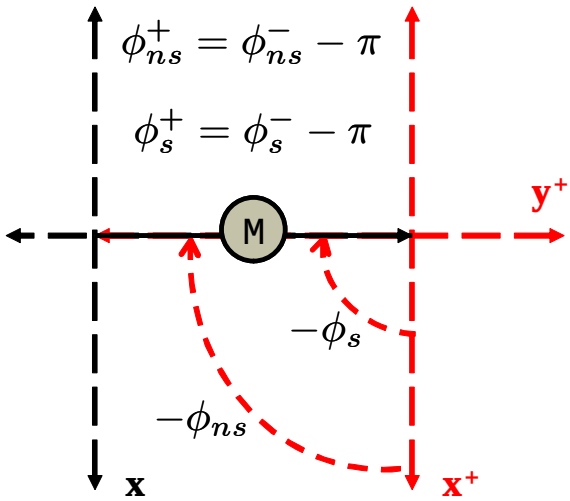

(f) Foot impact, legs switched

Figure 4. The stages of a divider-gait biped walking along the y-axis (top-down view, leg masses omitted)

2.4.4 Fix $\phi_{ns}(t) = \phi_s(t)$

This simplification results in bipedal walking like that of a rotating divider (or scissors). This style of walking is not human-like, as can be seen in the step progression of Fig. 4. The constraint $\phi_{ns}(t) = \phi_s(t)$ also implies that $\dot{\phi}_{ns}(t) = \dot{\phi}_s(t)$, and applying these two relations to the Lagrangian, we find two cyclic variables: ϕ_{ns} and ϕ_s. The simplified Lagrangian is found in Appendix (31). Moreover, the simplified matrix $M(\theta)$ is symmetric:

$$M_s(\theta) = \begin{pmatrix} M_1(\theta) & 0 \\ 0 & M_2(\theta) \end{pmatrix} \tag{10}$$

where $\theta = \begin{pmatrix} \theta_{ns} & \theta_s \end{pmatrix}^T$ and the symmetric submatrices $M_1(\theta)$ and $M_2(\theta)$ are given in Appendix (32, 33).

In the next section, we will use these properties to eliminate the ϕ time-derivatives and thus reduce the system into two dimensions (the sagittal plane).

2.5 Routhian Reduction

Now that we have a simplified Lagrangian with cyclic variables, we use Routhian reduction to exploit symmetries in the system. It should be noted that the cause of system symmetry is not the symmetric trait of matrix $M_s(\theta)$, but rather the absence of any ϕ angular positions within the matrix.

The Routhian is obtained by conserving certain quantities in the Lagrangian [16]. Specifically, we set

$$r = \frac{\partial L_s(\theta, \dot{\theta}, \dot{\phi})}{\partial \dot{\phi}} = M_2(\theta)\dot{\phi} \tag{11}$$

where r is a vector of constants; these are values that are assigned to the conserved quantities. Solving for $\dot{\phi}$ in terms of r, we obtain the Routhian given by

$$R(\theta, \dot{\theta}) = L_s(\theta, \dot{\theta}, M_2(\theta)^{-1}r) - r^T M_2(\theta)^{-1} r \tag{12}$$

In this case, because $\phi_{ns} = \phi_s$ (thus we have only one unique variable $\dot{\phi}$), the matrix $M_2(\theta)$ simplifies to a scalar function, $m_2(\theta)$, and the Routhian vector is replaced by a single constant, c. Therefore, the single $\dot{\phi}$ term is represented by the one-dimensional relation:

$$\dot{\phi} = \frac{c}{m_2(\theta)} \tag{13}$$

where

$$m_2(\theta) = b^2 m \sin(\theta_{ns})^2 - 2b(a+b)m \sin(\theta_{ns})\sin(\theta_s) + ((2a^2 + 2ab + b^2)m + (a+b)^2 M)\sin(\theta_s)^2$$

Using the expressions of (12),(23), and (31), the Routhian in terms of (13), (22), and (32) is

$$R(\theta, \dot{\theta}) = \frac{1}{2}\dot{\theta}^T M_1(\theta)\dot{\theta} - V(\theta) - \frac{c^2}{2m_2(\theta)} \tag{14}$$

Now that we have the Routhian in terms of known components, the reduced system of equations is derived using the definition of Lagrange (6). The proof that a Routhian holds as a Lagrangian is in Appendix B.1.

3 REDUCED MODEL

3.1 Equations of Motion

The reduced system of equations, now two-dimensional, is

$$ma^2(M_r(\theta)\ddot{\theta} + F_r(\theta,\dot{\theta})\dot{\theta} + \frac{1}{a}g_r(\theta) + \frac{1}{m^2a^4}\text{aug}(\theta)) = 0 \tag{15}$$

with the normalized components given in A.4. Matrices $M_r(\theta)$ and $F_r(\theta)$ are 2×2 and vectors $g_r(\theta)$ and $\text{aug}(\theta)$ are 2×1. The first three components describe the same terms as mentioned before, and in fact they are identical to the components of the original 2D model introduced in 1.2.1 [9]. The new vector $\text{aug}(\theta)$ contains the augmented terms of the Routhian reduction. An interesting observation is that the reduced system loses its leg-mass generality because of the augmented component. This vector is only dependent on θ, so the reduced 2D system can be thought of as the original 2D system with an augmented gravitational torque component.

The reduced system also has an additional parameter, the Routhian constant c. This constant describes the degree of influence of the conserved quantity. That is, a small c results in small arcs in the lateral plane, whereas a large c creates kicking swings. Moreover, when c is set to zero (no lateral motion), the augmented term disappears as expected, and we are left with the original 2D model. Therefore, the reduced model is a generalization of the original 2D model. This is significant because the reduced model is uniquely brought back into three dimensions in the next section. We have found a generalized two-dimensional system that describes both the 3D and 2D walker.

3.2 Three-Dimensional Reconstruction

Using the Routhian relation from (11), we can reconstruct the angular velocity of ϕ in terms of θ:

$$\dot{\phi}(t) = \frac{c}{m_2(\theta)} \tag{16}$$

From this, the angular position of the conserved quantity is easily calculated:

$$\phi(t) = \phi_{t_0} + \int_{t_0}^{t} \dot{\phi}(\tau)d\tau \tag{17}$$

where ϕ_{t_0} is the starting angular position at time t_0.

Since we are dealing with a third dimension, the reduced transition map is no longer sufficient. The original map T_r (5) is still used to reset the θ variables, but additional transition rules are needed for ϕ. The angular velocity $\dot{\phi}$ holds through impact because it is dependent on θ, which is reset. When the legs switch at collision, the angular positions of ϕ are not simply flipped as with the θ variables. This would do nothing considering that they are constrained to be equal. Instead, ϕ is bound by the following transition rule:

$$\phi^+ = \phi^- - \pi \tag{18}$$

This transition is shown in Fig. 4(f).

The reconstructed 3D model is unique because of its dependence on a model that we already know to be unique. As noted beforehand, the reduced model is the original 2D model with an augmented component. If the original 2D model is unique (by definition, it is derived uniquely), then that part of the reduced model is unique. Furthermore, the augmented component and the lateral plane expressions are dependent on the variables of θ from the 2D model. If θ is guided by a unique model, then the 3D parts are unique as well.

3.3 Limit Cycles in Three Dimensions

Limit cycles are periodic solutions for the hybrid system of a bipedal walker. The goal of this reduction from 3D to 2D is to facilitate previously established analytical techniques, such as searching the phase space for limit cycles. Now that we have a reduced model reconstructed into 3D, we can find hybrid solutions that also correspond to solutions for the higher-order (simplified) 3D model. The proof of this direct mapping is given in Appendix B.2. However, proving that there exists a hybrid solution that is *periodic* for both the reduced and higher-order models is not straight-forward, so we support this claim in the next section.

4 SIMULATION AND RESULTS

With the help of Simon Ng and Haiyang Zheng, we implemented our reconstructed hybrid system in HyVisual (hybrid dynamics) and parent platform Ptolemy II with GR domain (animation) [20, 2, 3]. Using this continuous-time and discrete-event modeler with custom actors [15], we implemented an algorithm to iterate over the discretized feasible state space to find initial conditions that correspond to stable limit cycles.

First, we established the parameters of the robot:

- $\gamma = \frac{\pi}{45} = 4^\circ$
- $\mu = 2.0$
- $\beta = 1.0$
- $a = 0.5$
- $g = 9.8$

The selection of leg mass m and Routhian constant c required more thought. After testing the reduced model with $m = 5$ and non-zero c, we discovered that the limit cycle's basin of attraction is far thinner for small m. In other words, the robot is more sensitive to perturbations and prone to fall over. The motion-dampening inertial forces in the lateral plane are minimal, so the trajectory of the ϕ variables must be exact. For this reason, we chose m to be around 90, which significantly increased the walker's stability.

We kept c very small in order to generate human-like arcs in the lateral plane. Natural human walking has a slight rotation in the lateral in order to avoid scuffing against the stance leg and the ground. This is similar to the scuffing compensation of McGeer's passive straight-legged model [17]. In our simulations, $c \approx 0.01$.

In order to validate whether each configuration is a fixed-point on the Poincaré return map, we use the method proposed in [9]. For each set of initial conditions, the algorithm fires the HyVisual simulator over two steps (a complete cycle) and records the initial conditions at the beginning of the next cycle. The initial conditions are then perturbed and simulated, one at a time, and the results after a complete cycle are subtracted from the unperturbed cycle's results to make a difference matrix. The difference matrix is multiplied by the diagonal matrix of inverted perturbation values. The eigenvalues are calculated from the resulting matrix, and if the magnitudes are all strictly less than one, the initial configuration is on a limit cycle.

The initial conditions and parameters are simultaneously tuned to find periodicity in both planes. This is because a periodic cycle in the sagittal does not necessarily correspond to a periodic cycle in the lateral. The

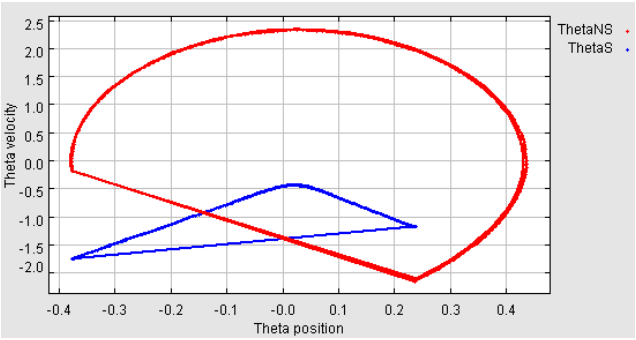

(a) Periodicity in the Sagittal Plane: $\theta(t)$ vs. $\dot{\theta}(t)$

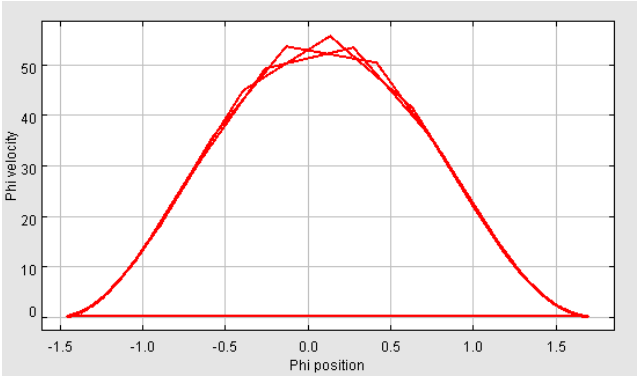

(b) Periodicity in the Lateral Plane: $\phi(t)$ vs. $\dot{\phi}(t)$

Figure 5. Limit cycle (m=89, c=0.01) in both planes

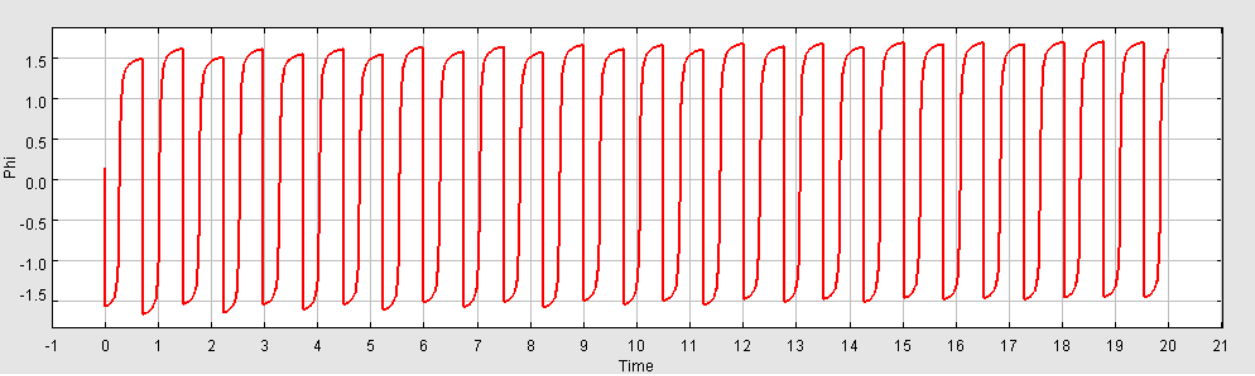

Figure 6. Periodic Evolution in the Lateral Plane (m=89, c=0.01): Time vs. $\phi(t)$

best configuration we found is with $c = 0.01$ and $m = 89$:

$$\begin{pmatrix} \theta_{ns}(t_0) \\ \theta_s(t_0) \\ \dot{\theta}_{ns}(t_0) \\ \dot{\theta}_s(t_0) \\ \phi(t_0) \end{pmatrix} = \begin{pmatrix} -0.3771 \\ 0.2061 \\ 0.15897 \\ -1.0667 \\ -\pi/2 \end{pmatrix}$$

This configuration resulted in a limit cycle in the sagittal plane (Fig. 5(a)) matching those found in [9] and [22]. Also, we indeed found periodicity in the ϕ variables, shown in Fig. 5(b). The timed evolution of angular position ϕ appears to be two-step periodic in Fig. 6, but we believe this to either be a discretization error or a sign that our c and m parameters are very close to one-step periodic values.

5 CONCLUSION AND FUTURE WORK

Even though the plots of this limit cycle are promising, we have not yet achieved natural walking behavior in a visualization. Currently, a 3D animation by Haiyang Zheng shows the swing leg rotating behind the x-z plane. That is, the swing leg never reaches stages (d)-(f) of Fig. 4, and instead goes back into the negative y region.

There are many subtleties about the reduced model that we do not yet understand. For example, because we do not have the full-order impact equations, we are unsure whether the θ variables can really carry ϕ over an impact. If our assumption is correct, there are symmetries in the impact equations just like the dynamics, but we cannot be positive until we visually confirm 3D walking.

Despite the remaining problems, we have successfully applied numerical analysis to the reduced model of a passive 3D biped. We have provided evidence of periodic 3D limit cycles, showing that 2D analytical techniques can be applied to 3D models through reduction. This research has demonstrated the promise of hybrid reduction, and much future work is necessary.

We still need to visually map periodic cycles for the reduced model into natural walking. Also, an application to powered robots is a next step that will test models of the form:

$$M(q)\ddot{q} + F(q,\dot{q})\dot{q} + g(q) + \text{aug}(q) = B(q)$$

where $B(q)$ is the matrix of actuation torques. We can more elegantly exploit the symmetries of dynamical systems. A generalization of hybrid reduction will allow analysis of different models and reduction without simplification constraints. We could potentially reduce a biped model with human-like strides, instead of the rotating divider motion of this paper's application. With all these topics to explore, we are certainly walking towards a greater understanding of three-dimensional bipeds.

5.1 Acknowledgements

First and foremost, I would like to extend my gratitude towards my mentor, Aaron D. Ames, for all his guidance and instruction. Dr. Jonathan Sprinkle's advice and support certainly contributed toward my advancement through the two-month research program. I could not have tested my work without the remarkable help of Haiyang Zheng, one of the pioneers of HyVisual. Also, I thank Simon Ng for implementing the reduced model in HyVisual. Finally, thank you to SUPERB, CHESS, and NSF for sponsoring my work over the summer.

A APPENDIX OF DYNAMICS EQUATIONS

A.1 Impact Equations

The following relationship exists between pre-impact and post-impact angular velocities in the sagittal plane [9]:

$$Q^-(\alpha)\dot{\theta}^- = Q^+(\alpha)\dot{\theta}^+$$

with the normalized forms of $Q^-(\alpha)$ and $Q^+(\alpha)$ being:

$$Q_n^-(\alpha) = ma^2 \begin{pmatrix} -\beta & -\beta + (\mu(1+\beta)^2 + 2(1+\beta))\cos(2\alpha) \\ 0 & -\beta \end{pmatrix}$$

$$Q_n^+(\alpha) = ma^2 \begin{pmatrix} \beta(\beta - (1+\beta)\cos(2\alpha)) & (1+\beta)((1+\beta) - \beta\cos(2\alpha)) + 1 + \mu(1+\beta)^2 \\ \beta^2 & -\beta(1+\beta)\cos(2\alpha) \end{pmatrix}$$

which describe the y-z plane's angular velocity transition map $H(\alpha)$:

$$H(\alpha) = Q_n^{+-1}(\alpha)Q_n^-(\alpha) \tag{19}$$

A.2 Original Full-Order Continuous Dynamics

The Lagrangian derivation begins with the position vectors of each point-mass on the robot. The time-derivatives of these yield the velocity vectors, which are used to determine the kinetic energy of the system:

$$K(q,\dot{q}) = \frac{1}{2}M||\vec{v_M}||^2 + \frac{1}{2}m||\vec{v_{ns}}||^2 + \frac{1}{2}m||\vec{v_s}||^2 \tag{20}$$

The kinetic energy expressed in terms of matrix $M(q)$ (25) is

$$K(q,\dot{q}) = \frac{1}{2}\dot{q}^T M(q)\dot{q} \tag{21}$$

Similarly, the potential energy is:

$$V(q) = V(\theta) = Mgl\cos(\theta_s) + mga\cos(\theta_s) + mg(l\cos(\theta_s) - b\cos(\theta_{ns})) \tag{22}$$

Finally, the Lagrangian is the difference:

$$L(q,\dot{q}) = K(q,\dot{q}) - V(q) = \frac{1}{2}\dot{q}^T M(q)\dot{q} - V(q) \tag{23}$$

$$\begin{aligned} L(q,\dot{q}) \;=\; & \frac{1}{2}(a^2 m(\sin(\theta_s)^2\dot{\phi}_s^2 + \dot{\theta}_s^2) + l^2 M(\sin(\theta_s)^2\dot{\phi}_s^2 + \dot{\theta}_s^2) \\ & + m((b\sin(\phi_{ns})\sin(\theta_{ns})\dot{\phi}_{ns} - l\sin(\phi_s)\sin(\theta_s)\dot{\phi}_s \\ & - b\cos(\phi_{ns})\cos(\theta_{ns})\dot{\theta}_{ns} + l\cos(\phi_s)\cos(\theta_s)\dot{\theta}_s)^2 \\ & + (b\cos(\phi_{ns})\sin(\theta_{ns})\dot{\phi}_{ns} - l\cos(\phi_s)\sin(\theta_s)\dot{\phi}_s + b\cos(\theta_{ns})\sin(\phi_{ns})\dot{\theta}_{ns} \\ & - l\cos(\theta_s)\sin(\phi_s)\dot{\theta}_s)^2 + (b\sin(\theta_{ns})\dot{\theta}_{ns} - l\sin(\theta_s)\dot{\theta}_s)^2)) \\ & + bgm\cos(\theta_{ns}) - agm\cos(\theta_s) - lg(M+m)\cos(\theta_s) \end{aligned} \tag{24}$$

Using the definition of Lagrange (6) to derive the equations of motion, we get the generalized system of (7), which has the following components (in terms of the normalized components):

$$M(q) = ma^2 M_n(q) \tag{25}$$

$$F(q,\dot{q}) = ma^2 F_n(q,\dot{q}) \tag{26}$$

$$g(q) = ma^2 g_n(q) \tag{27}$$

The normalized components are:

$$M_n(q) = \begin{pmatrix} M_n^{11} & M_n^{12} & M_n^{13} & M_n^{14} \\ M_n^{21} & M_n^{22} & M_n^{23} & M_n^{24} \\ M_n^{31} & M_n^{32} & M_n^{33} & M_n^{34} \\ M_n^{41} & M_n^{42} & M_n^{43} & M_n^{44} \end{pmatrix} \tag{28}$$

where matrix M_n has entries

$$\begin{aligned} M_n^{11} &= \beta^2 \\ M_n^{12} &= -(\beta+1)\beta(\cos(\phi_{ns}-\phi_s)\cos(\theta_{ns})\cos(\theta_s) + \sin(\theta_{ns})\sin(\theta_s)) \end{aligned}$$

$$
\begin{array}{ll}
M_n^{13} = 0 & M_n^{14} = -(\beta+1)\beta\cos(\theta_{ns})\sin(\phi_{ns}-\phi_s)\sin(\theta_s) \\
M_n^{21} = M_n^{12} & M_n^{22} = ((1+\beta)^2(\mu+1)+1) \\
M_n^{23} = (\beta+1)\beta\cos(\theta_s)\sin(\phi_{ns}-\phi_s)\sin(\theta_{ns}) & M_n^{24} = 0 \\
M_n^{31} = 0 & M_n^{32} = M_n^{23} \\
M_n^{33} = \beta^2\sin(\theta_{ns})^2 & M_n^{34} = -(\beta+1)\beta\cos(\phi_{ns}-\phi_s)\sin(\theta_{ns})\sin(\theta_s) \\
M_n^{41} = M_n^{14} & M_n^{42} = 0 \\
M_n^{43} = M_n^{34} & M_n^{44} = ((1+\beta)^2(\mu+1)+1)\sin(\theta_s)^2
\end{array}
$$

$$
F_n(q,\dot{q}) = \begin{pmatrix} F_n^{11} & F_n^{12} & F_n^{13} & F_n^{14} \\ F_n^{21} & F_n^{22} & F_n^{23} & F_n^{24} \\ F_n^{31} & F_n^{32} & F_n^{33} & F_n^{34} \\ F_n^{41} & F_n^{42} & F_n^{43} & F_n^{44} \end{pmatrix} \tag{29}
$$

where matrix F_n has entries

$$
\begin{array}{l}
F_n^{11} = 0 \\
F_n^{12} = (\beta+1)\beta(\cos(\phi_{ns}-\phi_s)\cos(\theta_{ns})\sin(\theta_s)\dot{\theta}_s - \cos(\theta_s)(\cos(\theta_{ns})\sin(\phi_{ns}-\phi_s)\dot{\phi}_s + sin(\theta_{ns})\dot{\theta}_s)) \\
F_n^{13} = -\frac{1}{2}\beta^2\sin(2\theta_{ns})\dot{\phi}_{ns} \\
F_n^{14} = (\beta+1)\beta\cos(\theta_{ns})(\cos(\phi_{ns}-\phi_s)\sin(\theta_s)\dot{\phi}_s - \cos(\theta_s)\sin(\phi_{ns}-\phi_s)\dot{\theta}_s) \\
F_n^{21} = ((\beta+1)\beta(\cos(\theta_{ns})\cos(\theta_s)\sin(\phi_{ns}-\phi_s)\dot{\phi}_{ns} + (\cos(\phi_{ns}-\phi_s)\cos(\theta_s)\sin(\theta_{ns}) - cos(\theta_{ns})\sin(\theta_s))\dot{\theta}_{ns})) \\
F_n^{22} = 0 \\
F_n^{23} = (\beta+1)\beta\cos(\theta_s)(\cos(\phi_{ns}-\phi_s)\sin(\theta_{ns})\dot{\phi}_{ns} + \cos(\theta_{ns})\sin(\phi_{ns}-\phi_s)\dot{\theta}_{ns}) \\
F_n^{24} = -\frac{1}{2}((\beta+1)^2(\mu+1)+1)\sin(2\theta_s)\dot{\phi}_s \\
F_n^{31} = \beta^2\cos(\theta_{ns})\sin(\theta_{ns})\dot{\phi}_{ns} \\
F_n^{32} = -(\beta+1)\beta\sin(\theta_{ns})(\cos(\phi_{ns}-\phi_s)\cos(\theta_s)\dot{\phi}_s + \sin(\theta_s)\sin(\phi_{ns}-\phi_s)\dot{\theta}_s) \\
F_n^{33} = \beta^2\cos(\theta_{ns})\sin(\theta_{ns})\dot{\theta}_{ns} \\
F_n^{34} = -(\beta+1)\beta\sin(\theta_{ns})(\sin(\phi_{ns}-\phi_s)\sin(\theta_s)\dot{\phi}_s + \cos(\theta_s)\cos(\phi_{ns}-\phi_s)\dot{\theta}_s) \\
F_n^{41} = -(\beta+1)\beta\sin(\theta_s)(\cos(\phi_{ns}-\phi_s)\cos(\theta_{ns})\dot{\phi}_{ns} - \sin(\theta_{ns})\sin(\phi_{ns}-\phi_s)\dot{\theta}_{ns}) \\
F_n^{42} = ((\beta+1)^2(\mu+1)+1)\cos(\theta_s)\sin(\theta_s)\dot{\phi}_s \\
F_n^{43} = (\beta+1)\beta\sin(\theta_s)(\sin(\phi_{ns}-\phi_s)\sin(\theta_{ns})\dot{\phi}_{ns} - \cos(\theta_{ns})\cos(\phi_{ns}-\phi_s)\dot{\theta}_{ns}) \\
F_n^{44} = ((\beta+1)^2(\mu+1)+1)\cos(\theta_s)\sin(\theta_s)\dot{\theta}_s
\end{array}
$$

$$
g_n(q) = \begin{pmatrix} \beta g\sin(\theta_{ns}) \\ -g((\beta+1)(\mu+1)+1)\sin(\theta_s) \\ 0 \\ 0 \end{pmatrix} \tag{30}
$$

A.3 Simplified Higher-Order Continuous Dynamics

The Lagrangian of the simplified, full-order 3D model is

$$
L_s(\theta,\dot{\theta},\dot{\phi}) \;=\; bmg\cos(\theta_{ns}) - g(b(m+M)+a(2m+M))\cos(\theta_s)
$$

$$
\begin{aligned}
&+\frac{1}{2}((b^2 m \sin(\theta_{ns})^2 - 2b(a+b)m\sin(\theta_{ns})\sin(\theta_s) \\
&+((2a^2+2ab+b^2)m + (a+b)^2 M)\sin(\theta_s)^2)\dot{\phi}_s^2 \\
&+b^2 m\theta_{ns}^2 - 2b(a+b)m\cos(\theta_{ns}-\theta_s)\dot{\theta}_{ns}\dot{\theta}_s \\
&+((2a^2+2ab+b^2)m + (a+b)^2 M)\dot{\theta}_s^2)
\end{aligned} \tag{31}
$$

Using this Lagrangian, the simplified kinematics component $M_s(\theta)$ (10) is derived with submatrices:

$$
M_1(\theta) = ma^2 \begin{pmatrix} \beta^2 & -\beta(1+\beta)\cos(\theta_{ns}-\theta_s) \\ -\beta(1+\beta)\cos(\theta_{ns}-\theta_s) & 1+(1+\beta)^2(1+\mu) \end{pmatrix} \tag{32}
$$

$$
M_2(\theta) = ma^2 \begin{pmatrix} \beta^2\sin(\theta_{ns})^2 & -\beta(1+\beta)\sin(\theta_{ns})\sin(\theta_s) \\ -\beta(1+\beta)\sin(\theta_{ns})\sin(\theta_s) & (1+(1+\beta)^2(1+\mu))\sin(\theta_s)^2 \end{pmatrix} \tag{33}
$$

A.4 Reduced Continuous Dynamics

The normalized components of the reduced system (15) are given by:

$$
M_r(\theta) = \begin{pmatrix} \beta^2 & -\beta(1+\beta)\cos(\theta_{ns}-\theta_s) \\ -\beta(1+\beta)\cos(\theta_{ns}-\theta_s) & 1+(1+\beta)^2(1+\mu) \end{pmatrix} \tag{34}
$$

$$
F_r(\theta,\dot{\theta}) = \begin{pmatrix} 0 & -\beta(1+\beta)\sin(\theta_{ns}-\theta_s)\dot{\theta}_s \\ \beta(1+\beta)\sin(\theta_{ns}-\theta_s)\dot{\theta}_{ns} & 0 \end{pmatrix} \tag{35}
$$

$$
g_r(\theta) = \begin{pmatrix} g\beta\sin(\theta_{ns}) \\ -g(1+(1+\beta)(1+\mu))\sin(\theta_s) \end{pmatrix} \tag{36}
$$

$$
\mathrm{aug}(\theta) = \begin{pmatrix} \frac{c^2\beta\cos(\theta_{ns})(-\beta\sin(\theta_{ns})+(1+\beta)\sin(\theta_s))}{\mathrm{denom}} \\ \frac{c^2\cos(\theta_s)(\beta(1+\beta)\sin(\theta_{ns})-(1+(1+\beta)^2(1+\mu))\sin(\theta_s))}{\mathrm{denom}} \end{pmatrix} \tag{37}
$$

where denom is the normalized form squared of $m_2(\theta)$:

$$
\mathrm{denom} = (\beta^2\sin(\theta_{ns})^2 - 2\beta(1+\beta)\sin(\theta_{ns})\sin(\theta_s) + (1+(1+\beta)^2(1+\mu))\sin(\theta_s)^2)^2
$$

B APPENDIX OF PROOFS

B.1 A Routhian holds as a Lagrangian

Lemma 1: If $L_s(\theta,\dot{\theta},\dot{\phi})$ is a Lagrangian by definition (6), then our Routhian $R(\theta,\dot{\theta})$ from (14) is a Lagrangian, i.e.:

$$
\frac{d}{dt}\frac{\partial R(\theta,\dot{\theta})}{\partial\dot{\theta}_i} - \frac{\partial R(\theta,\dot{\theta})}{\partial\theta_i} = 0, \forall i \in \{\mathrm{ns}, \mathrm{s}\} \tag{38}
$$

Proof: First, let us inspect our simplified higher-order Lagrangian (31). Because matrix $M_s(\theta)$ is symmetric, the Lagrangian can be written as

$$\begin{aligned} L_s(\theta, \dot{\theta}, \dot{\phi}) &= \frac{1}{2}\dot{q}^T M_s(\theta)\dot{q} - V(\theta) \\ &= \frac{1}{2}\dot{\theta}^T M_1(\theta)\dot{\theta} + \frac{1}{2}\dot{\phi}^T M_2(\theta)\dot{\phi} - V(\theta) \end{aligned} \tag{39}$$

Although our simplified model has a scalar term for $M_2(\theta)$, we will maintain the term's generality for this proof. Now, by applying the definition of Lagrangian to L_s, we get

$$\frac{d}{dt}\frac{\partial L_s(\theta, \dot{\theta}, \dot{\phi})}{\partial \dot{\theta}_i} - \frac{\partial L_s(\theta, \dot{\theta}, \dot{\phi})}{\partial \theta_i} = 0, \forall i \in \{\text{ns}, \text{s}\} \tag{40}$$

If our assumption holds, then the left-hand sides of both (38) and (40) are equal (ignoring index i):

$$\frac{d}{dt}\frac{\partial L_s(\theta, \dot{\theta}, \dot{\phi})}{\partial \dot{\theta}} - \frac{\partial L_s(\theta, \dot{\theta}, \dot{\phi})}{\partial \theta} = \frac{d}{dt}\frac{\partial R(\theta, \dot{\theta})}{\partial \dot{\theta}} - \frac{\partial R(\theta, \dot{\theta})}{\partial \theta}$$

Differentiation is a linear operation, so the $M_1(\theta)$ and $V(\theta)$ terms immediately cancel out. Multiplying both sides by two produces

$$\frac{\partial(\dot{\phi}^T M_2(\theta)\dot{\phi})}{\partial \theta} = \frac{\partial(r^T M_2^{-1}(\theta) r)}{\partial \theta}$$

Because we are conserving certain quantities with the Routhian relation (11), we have the expression:

$$r^T M_2^{-T}(\theta) r = r^T M_2^{-1}(\theta) r$$

Matrix $M_2(\theta)$ is symmetric, so $M_2^T(\theta) = M_2(\theta)$. Therefore, the expression is true, and the Routhian is a Lagrangian.

B.2 Solutions to the reduced model are solutions to the higher-order (simplified) model

Lemma 2: According to the definition of a hybrid system solution in (2), if $(\Phi_t^R, \tau^R, \chi^R)$ is a solution to the reduced hybrid system, then $(\Psi_t^L, \tau^L, \chi^L)$ is a solution to the higher-order hybrid system.

Proof: In order to prove this direct mapping, we must show that the solutions hold for both the continuous dynamics and the hybrid transition:

Lemma 2.1: If $\Phi_t^R(x_0)$, where $x = (\theta, \dot{\theta})^T$, is a solution for the reduced continuous dynamics, i.e.:

$$\frac{d}{dt}\frac{\partial R(\Phi_t^R(x_0))}{\partial \dot{\theta}_i} - \frac{\partial R(\Phi_t^R(x_0))}{\partial \theta_i} = 0, \forall i \in \{\text{ns}, \text{s}\}$$

then

$$\Psi_t^L(x_0) = \begin{pmatrix} \Phi_t^R(x_0) \\ \phi_{t_0} + \int_{t_0}^{t} \dot{\phi}(\tau) d\tau \\ \frac{c}{m_2(\theta)} \end{pmatrix} \tag{41}$$

is a solution to the higher-order continuous dynamics, i.e.:

$$\frac{d}{dt}\frac{\partial L_s(\Psi_t^L(x_0))}{\partial \dot{q}_i} - \frac{\partial L_s(\Psi_t^L(x_0))}{\partial q_i} = 0, \forall i \in \{\textbf{indices of all position states}\}$$

Proof: For $q_i = \theta_{ns}$ and $q_i = \theta_s$, the opposite direction of proof B.1 confirms that the definition of Lagrangian (6) holds. This cannot be used on $q_i = \phi$ because ϕ is not a defined variable in the Routhian. However, we know the following properties of $L_s(\theta, \dot{\theta}, \dot{\phi})$ from 2.4:

$$\frac{\partial L_s(\Psi_t^L(x_0))}{\partial \phi} = 0$$

From this, the definition of Lagrangian simplifies to

$$\frac{d}{dt}\frac{\partial L_s(\Psi_t^L(x_0))}{\partial \dot{\phi}} = 0$$

Moreover, from the definition of the Routhian (11):

$$\frac{\partial L_s(\Psi_t^L(x_0))}{\partial \dot{\phi}} = m_2(\theta)\dot{\phi} = c$$

Differentiation of a constant is zero, so the previous expression holds. Therefore, the solution to the reduced continuous dynamics is a solution to the higher-order continuous dynamics.

Lemma 2.2: If τ^R is the set of collision times for the reduced system, then τ^L is the set of collision times for the higher-order system.

Proof: Because the guard G from (1) is dependent only on θ, which by Lemma 2.1 holds through the higher-order dynamics, the collisions in the reduced model happen at the same time as the collisions in the higher-order model. Therefore, $\tau^R = \tau^L$.

Lemma 2.3: If $x_i \in \chi^R$ is

$$x_i = T^R(\Phi_{t_i}^R(x_{i-1}))$$

where $T^R(\theta, \dot{\theta})$ uses the reset map given in (5), then $y_i \in \chi^L$, defined by

$$y_i = \begin{pmatrix} x_i \\ \phi_{i-1} + \int_{t_{i-1}}^{t_i} \dot{\phi}(\tau)d\tau - \pi \\ \frac{c}{m_2(\theta)} \end{pmatrix} \tag{42}$$

is

$$y_i = T^L(\Psi_{t_i}^L(y_{i-1}))$$

where

$$T^L(\theta, \dot{\theta}, \phi, \dot{\phi}) = \begin{pmatrix} T^R(\theta, \dot{\theta}) \\ \phi^- - \pi \\ \frac{m_2(\theta^-)}{m_2(T_\theta^R(\theta^-))}\dot{\phi}^- \end{pmatrix} \tag{43}$$

Proof: Because of Lemma 2.1, we know that the flow $\Phi_t^R(x_i)$ maps to the flow $\Psi_t^L(x_i)$. Since x_i is contained in y_i, the reduced flow also maps to $\Psi_t^L(y_i)$. Also, because of Lemma 2.2, the impacts of both systems happen simultaneously. Thus, the higher-order flow produces pre-impact coordinates:

$$q^-(t_i) = \Psi_{t_i}^L(y_i)$$

where $q(t) = (\theta(t), \dot{\theta}(t), \phi(t), \dot{\phi}(t))^T$

Clearly, the θ and $\dot{\theta}$ terms of q^- hold through the higher-order transition since T^L (43) uses the same map on those terms as the reduced transition, T^R.

According to (41), q^- contains:

$$\phi^- = \phi_{i-1} + \int_{t_{i-1}}^{t_i} \dot{\phi}(\tau) d\tau$$

Applying this to the reset map T^L, we get the same term minus π, so ϕ holds through the transition.

Furthermore, q^- also contains:

$$\dot{\phi}^- = \frac{c}{m_2(\theta^-)}$$

When the system goes through the reset map T^L, the denominator of the $\dot{\phi}$ term cancels out, producing

$$\frac{c}{m_2(T_\theta^R(\theta^-))} = \frac{c}{m_2(\theta)}$$

which is the $\dot{\phi}$ term of y_i. Therefore, the higher-order coordinates hold through the transition.

Finally, because each part of a solution to the reduced system holds over the higher-order system's continuous dynamics and hybrid transitions, Lemma 2 is true.

References

[1] A. D. Ames and S. Sastry. A homology theory for hybrid systems: Hybrid homology. pages 86–105. HSCC LNCS 3414, 2005.

[2] C. Brooks, A. Cataldo, E. A. Lee, J. Liu, X. Liu, S. Neuendorffer, and H. Zheng. Hyvisual: A hybrid system visual modeler. Technical Report Technical Memorandum UCB/ERL M05/24, University of California, Berkeley, July 15 2005.

[3] C. Brooks, E. A. Lee, X. Liu, S. Neuendorffer, Y. Zhao, and H. Zheng. Heterogeneous concurrent modeling and design in java (volume 3: Ptolemy ii domains). Technical Report Technical Memorandum UCB/ERL M05/23, University of California, Berkeley, July 15 2005.

[4] M. Ceccarelli. *Fundamentals of mechanics of robotic manipulation.* Kluwer Academic Publishers, Boston, 2004.

[5] C. Chevallereau, E. R. Westervelt, and J. W. Grizzle. Asymptotic stabilization of a five-link, four-actuator, planar bipedal runner. Technical report, December 2004.

[6] M. J. Coleman. A stability study of a three-dimensional passive-dynamic model of human gait, February 1998.

[7] S. H. Collins, M. Wisse, and A. Ruina. A three-dimensional passive-dynamic walking robot with two legs and knees. *The International Journal of Robotics Research*, 20(7):607–615, July 2001.

[8] M. Garcia, A. Chatterjee, A. Ruina, and M. Coleman. The simplest walking model: Stability, complexity, and scaling. *ASME Journal of Biomechanical Engineering*, February 1998.

[9] A. Goswami, B. Thuilot, and B. Espiau. Compass-like biped robot: Part i: Stability and bifurcation of passive gaits. Technical report, INRIA Rhone-Alpes, France.

[10] J. W. Grizzle, G. Abba, and F. Plestan. Asymptotically stable walking for biped robots: Analysis via systems with impulse effects. IEEE TAC, February 1999.

[11] J. W. Grizzle, G. Abba, and F. Plestan. Proving asymptotic stability of a walking cycle for a five dof biped robot model. Clawar, 1999.

[12] I. A. Hiskens. Stability of hybrid system limit cycles: Application to the compass gait biped robot. IEEE Conference on Decision and Control, December 2001.

[13] Y. Hurmuzlu and D. B. Marghitu. Rigid body collisions of planar kinematic chains with multiple contact points. *The International Journal of Robotics Research*, 13(1):82–92, February 1994.

[14] A. D. Kuo. Stabilization of lateral motion in passive dynamic walking. *The International Journal of Robotics Research*, 18(9):917–930, 1999.

[15] E. A. Lee and H. Zheng. Operational semantics of hybrid systems. Zurich, Switzerland, March 9-11 2005. HSCC LNCS TBD.

[16] J. E. Marsden and R. T. S. *Introduction to Mechanics and Symmetry*. Springer, 2 edition, 2002.

[17] T. McGeer. Passive dynamic walking. *The International Journal of Robotics Research*, 9(2):62–82, 1990.

[18] S. Miyakoshi and G. Cheng. Examining human walking characteristics with a telescopic compass-like biped walker model. Japan, 2004. IEEE.

[19] R. M. Murray, L. Zexiang, and S. Sastry. *A mathematical introduction to robotic manipulation*. CRC Press, Boca Raton, 1994.

[20] S. Ng and H. Zheng. Model, simulation, and analysis of a bipedal walker. Technical report, University of California, Berkeley, July 2005. SUPERB-IT.

[21] M. W. Spong. The passivity paradigm in the control of bipedal robots. Technical report, University of Illinois at Urbana-Champaign.

[22] M. W. Spong and G. Bhatia. Further results on control of the compass gait biped. Technical report, University of Illinois at Urbana-Champaign.

[23] M. W. Spong and F. Bullo. Controlled symmetries and passive walking. Technical report, University of Illinois at Urbana-Champaign.